Published in AJSE, Vol:22, Issue: 2
Received on 16th September 2022
Revised on 3rd January 2023
Accepted on 30th June 2023

AIUB JOURNAL OF SCIENCE AND ENGINEERING
ISSN: 1608 – 3679 (print) 2520 – 4890 (Online)

Time Multiplexed Optical-OFDMA for Uplink Transmission in LiFi-based IoT Networks

Md Jahid Hasan, *Member, IEEE,* Ikenna Chinazaekpere Ijeh, *Member, IEEE,* Oussama Haddad, and Md Abdur Rahman, *Senior Member, IEEE*

***Abstract*—The transfer of data from multiple internet of things (IoT) devices requires the use of a robust and efficient multiple access (MA) solution. This paper considers the orthogonal frequency division MA (OFDMA) technique for the light-fidelity (LiFi)-based IoT uplink using infrared to transmit data from multiple mobile users to a fixed access point. The conventional schemes based on orthogonal frequency allocate distinct subcarriers to each user sharing the same time slot. We consider a new approach by allocating distinct time slots to a group of OFDMA users. Taking into account realistic opto-electronic components, we study the performance of the conventional and proposed optical-OFDMA schemes. We show that asymmetrically clipped optical-OFDMA signaling scheme outperforms direct current biased signaling in terms of electrical power efficiency. Focusing on the asymmetrically clipped signaling, we demonstrate the robustness of our proposed time multiplexed optical-OFDMA scheme against MA interference caused by signal clipping. We also show the advantages of our scheme in reducing computational complexity by a factor of 2 compared to the conventional optical-OFDMA schemes.**

***Index Terms*—Light-fidelity; optical wireless communications; internet of things; multiple access; OFDMA.**

I. Introduction

The internet has already transformed our way of life and become an integral part of almost everything we do today. The astounding growth of internet-based ubiquitous connectivity is predominantly driven by instant mobile communication devices, e.g., smartphones, tablets, and laptops. Majority of these devices access the internet through the use of WiFi (wireless fidelity) technology relies on license-free industrial, scientific and medical (ISM) radio band. Moreover, billions of internet of things (IoT) and internet of medical things (IoMT) devices share the ISM and licensed ultra wide bands [1, 2, 3], resulting in spectrum congestion and increased electromagnetic interference (EMI). Therefore, an alternative to the existing radio frequency (RF) is required to ensure uninterrupted internet connectivity. Light-based optical wireless networking solutions, such as light fidelity (LiFi), have emerged as a complementary approach to the existing RF technology [4].

A. Light-based Indoor Connectivity

LiFi is a bidirectional short-range optical wireless communication (OWC) technology that is considered to be one of the key enabling technologies for future 6G networks, in particular for indoor applications. It may employ both visible and invisible (e.g., infrared, ultraviolet) lights, where the former refers to visible light communication (VLC) [5, 6, 7]. Light-based communication has several advantages compared to its RF counterparts, e.g., availability of license-free unregulated spectrum, immunity to electromagnetic interference, high-speed connectivity, and low latency [4, 8]. Moreover, LiFi offers unique physical security against eavesdropping and data theft, as lights do not penetrate opaque walls.

In this paper, we investigate the application of LiFi for mobile IoT devices and focus on the uplink data transmission, i.e., the transfer of data from the IoT devices to a ceiling-mounted access point (AP). Here, we consider employing invisible light, i.e., infrared (IR), in order to avoid visual irritation that may result in the VLC uplink. Of course, VLC could be used in the downlink (i.e., from the ceiling-mounted AP to the mobile devices), supporting both illumination and communication simultaneously. Also, this avoids the interference between the uplink and downlink transmissions. However, due to the possible eye hazard may cause by IR, the IEC (International Electrotechnical Commission) standard imposes a limitation on the maximum transmit power [9]. Thankfully, commercially available light-emitting diodes (LEDs) now have a large surface area producing a wide beam, permitting the use of reasonably high optical transmit power.

B. Multiple Access Solutions

Typically, several IoT devices in an indoor scenario transmit their data simultaneously at the same time. This continuous data transfer is enabled by employing an efficient multiple access (MA) technique, where all the users share the same communication channel. MA techniques can be classified into two categories: orthogonal MA (OMA) and non-orthogonal MA (NOMA), where the former allocates distinct orthogonal resources to each user and the latter allows multiple users to share their allotted orthogonal resources [10, 11]. OMA

This work was funded by American Internation University-Bangaldesh through the faculty research grant.

Md Jahid Hasan is with the Department of Electrical and Electronic Engineering, American International University-Bangladesh, Dhaka 1229, Bangladesh. He is now on leave to conduct postdoctoral research at the University College Cork, Tyndall National Institute, Cork, Ireland (e-mail: jahid.hasan@tyndall.ie).

Ikenna Chinazaekpere Ijeh is with the Department of Electrical and Electronic Engineering, Alex-Ekwueme Federal University Ndufu-Alike Ikwo, Ebonyi State, Nigeria (email: ikenna.ijeh@funai.edu.ng).

Oussama Haddad is with the Microelectronics and Telecommunications Department of Polytech-Marseille, Institut Fresnel, Marseille, France (email: oussama@fresnel.fr).

Md Abdur Rahman is with the Department of Electrical and Electronic Engineering, American Internation University-Bangaldesh, Dhaka 1229, Bangladesh (email: arahman@aiub.edu).

schemes such as time-division MA (TDMA) and code-division MA (CDMA) have been considered in several multi-user OWC applications, where the requirement of high data-rate is not so stringent [12, 13, 14, 15, 16]. However, with the increasing data-rate and the number of users, they suffer from increased implementation complexity due to the multi-user timing synchronization needed in TDMA and longer spreading sequence in CDMA. In order to address these issues power-domain (PD) NOMA has been proposed for LiFi based IoT networks [17]. In the PD-NOMA, each user is assigned a distinct power level, and multi-user detection (e.g., successive interference cancellation, SIC) is performed at the receiver (Rx) on the aggregate received signal based on the channel gains of each user [18]. Therefore, performance is highly affected by the correlations of users' received signal power. This is typically the case for the LiFi uplink scenarios for users with IoT devices in close proximity and mobility. Additionally, SIC receivers suffer from relatively high computational complexity. On the other hand, code-domain NOMA techniques share spreading sequences among multiple users at the expense of increased decoding complexity at the receiver, in particular, with the increased number of users [19].

C. Orthogonal Frequency Division MA Technique

Optical orthogonal frequency division MA (O-OFDMA) is a popular bandwidth-efficient multi-user version of the optical orthogonal frequency division multiplexing (O-OFDM) because of its robustness against the frequency-selective fading channel [20]. Considering the intensity modulation and direct detection (IM/DD) in the optical transmission, only the real-valued positive "time-domain" (TD) signal is transmitted. In contrast to the traditional RF OFDMA, Hermitian Symmetry (HS) is first imposed on the "frequency-domain" (FD) signal of the O-OFDMA to construct a real-valued TD signal. Then, to satisfy the LED's positive signaling requirement, a DC bias could be applied to the real-valued TD signal, known as DC-biased O-OFDMA (DCO-OFDMA) [21]. Alternatively, modulating only the odd subcarriers followed by zero clipping the negative TD signals can also be used, referred to as asymmetrically clipped O-OFDMA (ACO-OFDMA) [22].

One major issue of O-OFDMA is the relatively high peak-to-average power ratio (PAPR), resulting in further clipping (modelled as so-called "clipping noise") the signal in order to limit the signal peaks in the LED dynamic range (DR). Moreover, clipping the TD signal limits the power consumption of power amplifiers, but at the cost of performance degradation [23]. The reduction of clipping noise so far has relied on techniques, such as block coding, selective mapping, and pilot-assisted transmission [24, 25]. However, as shown in [23], for relatively low modulation order, clipping noise has a marginal degrading effect.

We consider here the O-OFDMA scheme because of the relatively large transmission bandwidth (BW) required in an indoor LiFi-based IoT scenario. Power consumption in battery-powered IoT devices is crucial, which is related to the transmit optical power and the computational complexity. Compared to OFDMA, another alternative approach is single-carrier FDMA (SCFDMA), which is widely used in the LTE (Long-Term Evolution) uplink due to its low PAPR [26]. However, the additional discrete Fourier Transform (DFT) pre-coding and filtering at the SCFDMA transmitter (Tx), results in relatively high computational complexity [23].

D. Proposed MA Scheme and Contributions

In this work, we study the performance of O-OFDMA scheme and compare the ACO and DCO signaling when used for LiFi-based IoT uplinks. We take into account a realistic LED model and analyze the performance in terms of power efficiency and MA interference (MAI) effect. Furthermore, we propose a MA technique called time multiplexed O-OFDMA (TMO-OFDMA), where we perform TDMA scheduling among a group of O-OFDMA users, which is done for the first time within the context to the best of our knowledge. Focusing on the proposed TMO-OFDMA scheme based on ACO signaling called "TM-ACO-OFDMA", we show the advantage of the scheme to manage MAI and computational complexity.

The main contributions of this work are:

- Studying the O-OFDMA performance for the LiFi uplink IoT networks in an indoor scenario;
- Showing the advantage of ACO signaling in terms of electrical power efficiency, as compared to DCO signaling;
- Proposing the time multiplexed O-OFDMA scheme by TDMA scheduling of O-OFDMA-based users;
- Performance comparison of the proposed TMO-OFDMA scheme with O-OFDMA taking into account realistic opto-electronic front-ends;
- Elucidating the advantage of our proposed scheme in reducing MAI and the computational complexity.

The remainder of the paper is organized as follows. In Section II, we present the system descriptions of the LiFi-based IoT networks for an indoor scenario. Next, Section III presents the considered MA schemes including the proposed TMO-OFDMA scheme. Afterwards, Sections IV and V investigate the performance and computational complexity of the schemes, respectively. Lastly, Section VI concludes the paper with some research directions for the future.

Notations : $.^*$ and $\ln(\cdot)$ refer to the complex conjugate and natural logarithm, respectively. $E\{\cdot\}$ stands for the expected value.

II. System Description

A. General Assumption

Figure 1 illustrates a typical LiFi uplink indoor scenario, where potentially up-to sixteen users, each one having a single LiFi-enabled IoT device, transmit data by using IR to an AP placed on the ceiling. Note that, in this sequel we use "IoT" and "IoMT" terms interchangeably.

In order to focus on the performance of the MA scheme, we consider a single-cell network architecture with a single AP. Note that, a single-cell [13] or a multi-cell [27] architecture may use several APs to cover a larger space. IoT devices (i.e.,

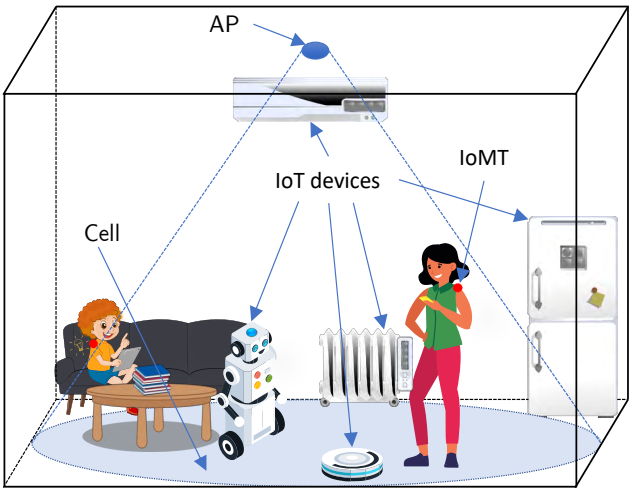

Fig. 1: Illustration of a LiFi uplink scenario in an indoor environment for multiple users, each one with a LiFi-enabled IoT device by using IR. IoMT devices are placed on the users' shoulder (the red bullet) and a single AP is placed on the ceiling.

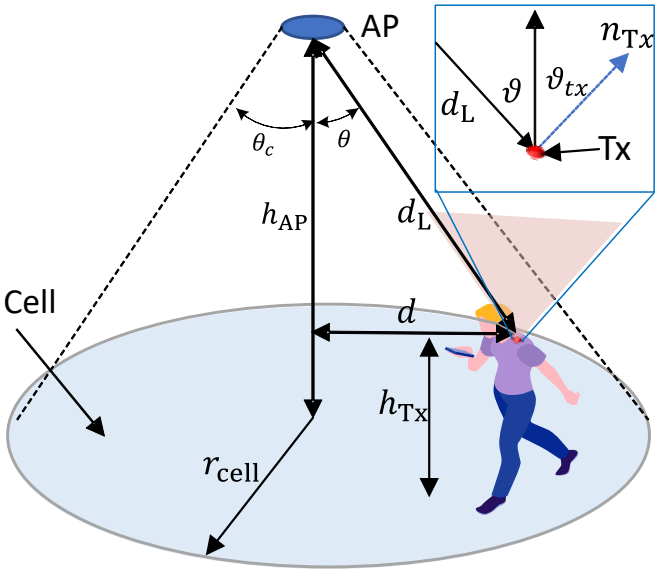

Fig. 2: Illustration of the LOS link distance between the AP and the Tx. Here, r_{cell} corresponding to the cell radius.

the Txs) are assumed to be transmitted at a rate of 1 Mbps, which satisfies the data-rate requirement of most IoT and IoMT devices, e.g., refrigerators, helping robots, room heaters, vacuum cleaner robots, and health monitoring sensors [28, 29].

At the Rx (i.e., the AP) side, a simple PIN photo-detector (PD) with a relatively large field-of-view (FOV) is considered to cover a larger area and no optical concentrator, which ensures less sensitivity to background noise (i.e., ambient noise), as compared to avalanche PD.

At the Tx side, we consider each IoT device is equipped with an IR LED of a relatively wide beam due to the eye-safety concern. Note that, according to the IEC standard, an IR exposure limit of $100\,\mathrm{W/m^2}$ poses no risk to the human eyes [9]. Here, we consider a Lumiled IR LED of wavelength 850 nm [30], which meets the requirements of eye-safety standard.

We assume perfect time synchronization for each mobile IoT device with the AP. Note that the error in time synchronization is a recurrent problem for OFDMA-based schemes, which is relatively low for an indoor scenario due to the limited mobility of the mobile users [31]. Also, in order to avoid MAI and so-called "near-far problems", both time and frequency synchronization is required for the RF OFDMA, typically referred as *initial ranging* [32]. However, the inherent absence of a carrier eliminates the need for frequency synchronization in O-OFDMA. Moreover, most timing synchronization methods in the literature rely on obtaining channel state information (CSI) by transmitting training sequences [33, 34, 35, 36]. Training sequences from each mobile device are typically sent via the uplink to the AP; based on the received signal, the CSI is estimated at the AP and transmitted via the downlink to the mobile devices [23]. Here, we assume a perfect estimation of the CSI at the AP for each mobile IoT device.

B. Channel Model

Similar to the radio channel, the propagation channel for light communication includes both line-of-sight (LOS) and non-LOS transmissions [37]. However, for the sake of simulation simplicity and in order to fous on the MA scheme, we consider only LOS link and neglect the non-LOS contribution. As a matter of fact, OWC heavily relies on the contributions from the LOS link, in particular near to the center of the cell [23]. Considering a Lambertian LED model at the Tx, the channel DC gain H_{LOS} for the LOS link is given by [38]:

$$H_{\text{LOS}} = \begin{cases} \frac{A_{\text{PD}}(m+1)}{2\pi d_{\text{L}}^2} \cos^m(\vartheta)\cos(\theta) & ;\, 0 \le \theta \le \theta_c \\ 0 & ;\, \theta > \theta_c, \end{cases} \tag{1}$$

where A_{PD} refers to the PD's active area, θ denotes the beam incident angle at the AP (i.e., the Rx), and θ_{c} is the FOV of the Rx. Also, ϑ is the Tx radiance angle that relies on Tx orientation angle ϑ_{tx}, as shown in Fig. 2. Here, d_{L} stands for the LOS link distance between the Tx and the AP, given by $d_{\text{L}} = \sqrt{d^2 + h_{\text{AP}}^2 - h_{\text{Tx}}^2}$, where h_{AP} and h_{Tx} are the heights of the AP and the Tx, respectively. Also, d is the horizontal distance between the Tx and the AP (i.e., the cell center)(see Fig. 2). Moreover, m in (1) stands for the Lambertian order given by [39]:

$$m = \frac{-\ln 2}{\ln(\cos\varphi_{1/2})}, \tag{2}$$

where $\varphi_{1/2}$ is the LED semi-angle at half power. Denoting the transmit optical power by $P_{\mathcal{T}(\text{opt})}$ and the PD responsivity by $\Re$, the received photo-current at the PD is [7]:

$$i_r = \Re H_{\text{LOS}} P_{\mathcal{T}(\text{opt})}. \tag{3}$$

Considering the load resistance R_L of the trans-impedance amplifier (TIA), the electrical power P_r at the receiver is:

$$P_r = i_r^2 R_L. \tag{4}$$

For the case of PIN PD, the noise sources at the AP consist of thermal and background noises, which are modeled as zero-mean white Gaussian with one sided power spectral density $\mathcal{N}_0$ [40]:

$$\mathcal{N}_0 = 4K_B T/R_L + 2q_e I_b, \tag{5}$$

where T stands for the temperature, K_B is the Boltzmann's constant, q_e refers to the electron charge, and I_b denotes the background noise.

III. Considered MA Schemes

In this section, we first present the conventional O-OFDMA scheme for both DCO and ACO signaling. Then we describe our proposed TMO-OFDMA scheme.

A. DCO-OFDMA

Figure 3 represents the block diagram of DCO-OFMDA scheme. First, the transmitted data bits from each IoT devices are grouped together by the serial to parallel (S/P) converter and mapped into complex M-QAM symbols χ_k, $k = 0, 1 \cdots, \mathscr{M} - 1$, where $\mathscr{M}$ refers to the number of sub-carriers per user (i.e., the IoT device). Denoting the number of users by Γ, total number of sub-carriers $\mathcal{M} = \mathscr{M}\Gamma$, which are mapped into symbols $\tilde{\chi}_{\tilde{k}}$, $\tilde{k} = 0, 1, \ldots, \mathcal{M}-1$, by employing a sub-carrier mapping technique. Note that the sub-carrier mapping techniques are classified into interleaved, distributed, and localized mapping [23]. We will later present the considered sub-carrier mapping technique in Section IV-A. Then, a real-valued TD signal is attained by imposing HS constraint on the mapped sub-carriers $\tilde{\chi}_{\tilde{k}}$ to get $\breve{\chi}_{\breve{k}}$, $\breve{k} = 0, 1, \ldots, N-1$; $N = 2\mathcal{M} + 2$, such that,

$$\breve{\chi}_{\breve{k}} = \Big[0, \chi_0, \chi_1, \ldots, \chi_{\mathcal{M}-1}, 0, \chi^*_{\mathcal{M}-1} \ldots, \chi^*_0\Big].$$

Next, the inverse fast Fourier transform (IFFT) is performed on the HS constrained symbols $\breve{\chi}_{\breve{k}}$ to obtain real-valued TD signal $\hat{x}_n$:

$$\hat{x}_n = \frac{1}{\sqrt{N}} \sum_{\breve{k}=0}^{N-1} \breve{X}_{\breve{k}} \exp\left(j\frac{2\pi n\breve{k}}{N}\right);\ n = 0, 1, \ldots, N-1. \tag{6}$$

The TD signal is then passed through the parallel to serial (P/S) converter and a cyclic prefix (CP) of length N_{CP} is appended at the end of the signal. After that, the resulting signal is converted into digital signal by a digital-to-analog converter (DAC) and amplified by an amplifier (AMP) before applying a DC bias $\mathscr{B}_{\text{DC}}$ to obtain $\breve{x}_n$:

$$\breve{x}_n = \tilde{x}_n + \mathscr{B}_{\text{DC}}, \tag{7}$$

where $\tilde{x}_n$ refers to the signal after the amplification. Lastly, upper and lower clipping is applied on the signal $\breve{x}_n$ and the LED is driven by the resulting signal x_n.

At the Rx, after the photo-detection at the PD, the DC bias is removed from the converted electrical signal and then amplified by a trans-impedance amplifier (TIA). The amplified signal is then converted into a discrete time signal r_n by an analog to digital converter (ADC). Next, after removing the CP, the signal is passed through a S/P converter and N-point fast-Fourier-transform (FFT) is performed, resulting in:

$$\breve{\zeta}_n = \frac{1}{\sqrt{N}} \sum_{n=0}^{N-1} r_n \exp\left(j\frac{2\pi n\breve{k}}{N}\right);\ \breve{k} = 0, 1, \ldots, N-1. \tag{8}$$

Afterwards, HS constrain is removed from the signal $\breve{\zeta}_{\breve{k}}$ and a single tap equalization is performed on the resulting signal $\tilde{\zeta}_{\tilde{k}}$. Finally, after sub-carrier demapping, QAM demodulation is done on the symbols ζ_k and transmitted serial data are recovered after the parallel to serial (P/S) conversion.

B. ACO-OFDMA

ACO-OFDMA relies on the modulating only the odd sub-carriers for signal transmission. After imposing the HS constraint before the IFFT block, the symbols $\breve{\chi}_{\breve{k}}$ has the following structure:

$$\breve{\chi}_{\breve{k}} = \Big[0, \chi_0, 0, \chi_1, \ldots, 0, \chi_{\mathcal{M}-1}, 0, \chi^*_{\mathcal{M}-1} \ldots, 0, \chi^*_0\Big].$$

After performing the IFFT, the negative signals are zero clipped without causing any error (i.e., loss of information) due to the anti-symmetry property of $\tilde{x}_n$ [21]. The rest of the steps are similar to those of DCO-OFDMA, as described in the previous subsection. Note that the ACO-OFDMA also requires the addition of a DC bias in order to fit the signal to the LED I-V characteristics [23], as will be clarified in the next subsection.

C. Proposed TMO-OFDMA Scheme

As mentioned earlier, in our proposed TMO-OFDMA scheme, TDMA scheduling is performed for a group of O-OFDMA-based users. A set of users transmit data during their allotted time window, as shown in Fig. 4. Here, considering the number of users $\Gamma = 12$, users are mapped into three different time slots for TMO-OFDMA. Each time-slot in TMO-OFDMA consists of 4 users transmitting data to their allocated time slots, unlike O-OFDMA, . To attain the same data rate as O-OFDMA, TMO-OFDMA users must finish their data transmissions within the same time frame as O-OFDMA. Denoting the total number of TMO-OFDMA slots by $\mathcal{N}$, each slot in TMO-OFDMA must transmit $\mathcal{N}$ times the rate of the conventional O-OFDMA scheme. Although, this will increase the required transmission BW of the system, we will show the advantage of our proposed scheme particularly for such low data-rate IoT applications later in Sections IV-C and V.

D. LED Characteristics and DC Bias Setting

Figure 5 shows the LED I-V characteristics curve of a typical low power Lumiled LED, HDN1102W-TR [41], that we consider here. In practice, regardless of the OFDMA signaling, a DC bias is added to the TD signal in order to fit it to the LED DR. We consider here the realistic non-linear characteristics of the LED, as shown in the Fig. 5 (the green

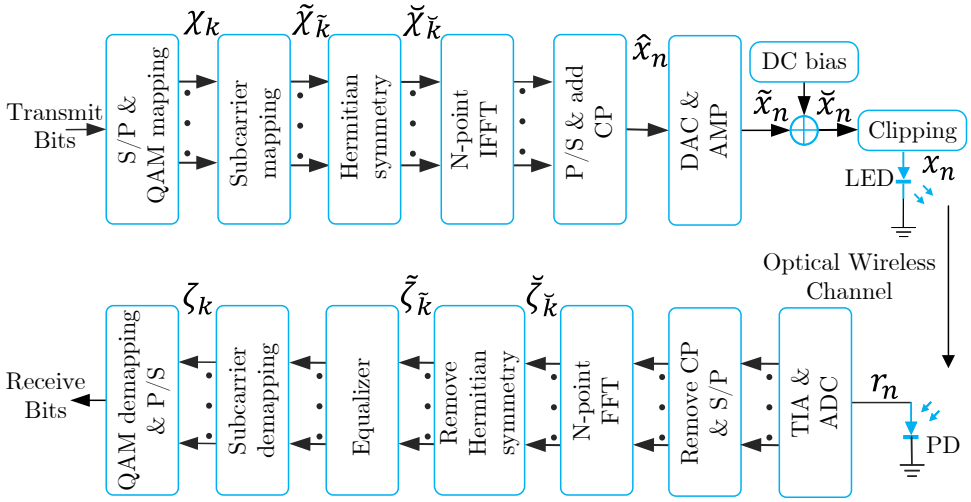

Fig. 3: Block diagram representation of the DCO-OFDMA signaling scheme.

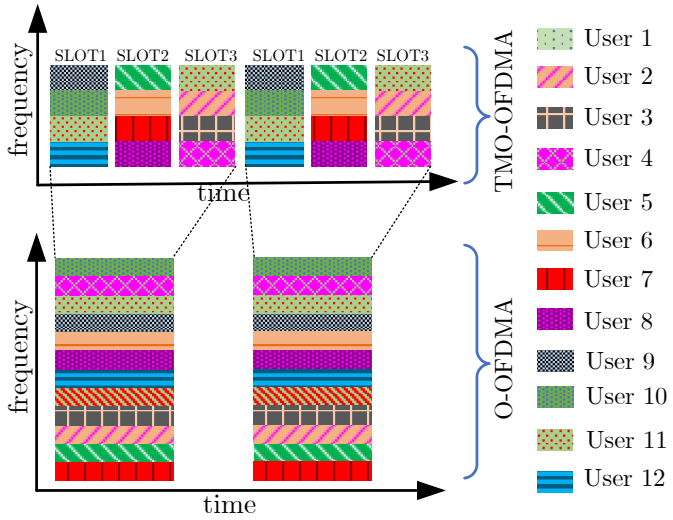

Fig. 4: Conceptual representation of the proposed TMO-OFDMA versus O-OFDMA for 12 users. Here, in TMO-OFDMA, users are allocated in 3 dedicated time slots.

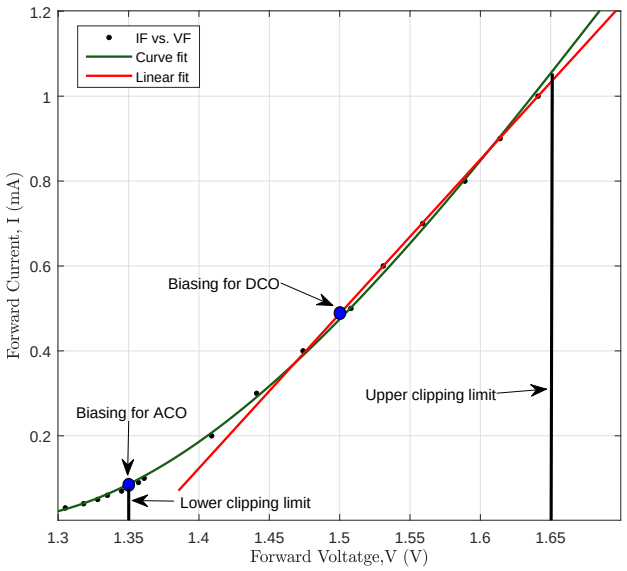

Fig. 5: LED I-V characteristics curve, HDN1102W-TR [41].

plot). We set the the DC bias $\mathscr{B}_{\text{DC}}$ at $1.5\,V$ for DCO signaling, i.e., the mid point between the upper and lower clipping bound. Also, the $\mathscr{B}_{\text{DC}}$ for ACO signaling is set to $1.35\,V$, which fits the signaling within the LED DR.

IV. Performance Analysis

In this section, we present numerical results to evaluate the performance of the conventional O-OFDMA and the proposed TMO-OFDMA schemes. First, we compare the performance of ACO and DCO signaling for O-OFDMA in terms of power efficiency and MAI effect. Then, we show the improvement in MAI effect of the TMO-OFDMA scheme, as compared with O-OFDMA.

A. Performance Parameters and Specifications

In a typical IoT-based indoor scenario, we consider the number of users $\Gamma = 16$, each with a data-rate of $\mathscr{R}_b = 1$ Mbps, as mentioned earlier. Also, unless otherwise specified, the total number of subcarriers $\mathcal{M} = 256$ and the number of subcarriers per user $\mathscr{M} = 16$. The other parameters are summarized in the Table I. Moreover, for the sake of simulation simplicity, if otherwise not stated, IoT devices are considered to point straight upward towards the ceiling, i.e., $\vartheta_{tx} = 0$ in Fig. 2. Here, we consider the interleaved subcarrier mapping, as illustrated in Fig. 6 for the case of two users.

We evaluate the bit-error-rate (BER) performance as a function of electrical signal-to-noise ratio (SNR) per bit $\mathscr{E}_{b(\text{elec})}/\mathscr{N}_o$ or the electrical transmit power $P_{\tau(elec)} = E\{x_n^2\}$,

TABLE I: Parameters Used for Numerical Simulations

Parameter	Symbol	Value
Tx height	h_{Tx}	0.4 m
AP height	h_{AP}	3 m
Cell radius	r_{cell}	3 m
Tx orientation angle	ϑ_{tx}	0
Max. Number of users	Γ	16
Data-rate per user	$\mathscr{R}_b$	1 Mbps
No. of mapped subcarriers	$\mathcal{M}$	256
Target BER	—	10^{-3}
LED wavelength [41]	λ	850 nm
LED semi-angle at half power	$\varphi_{1/2}$	60°
LED BW	—	40 MHz
Power conversion efficiency [41]	α	0.8
PD active area	A_{PD}	1 cm^2
PD responsivity	$\Re$	0.6 A/W
Rx FOV	θ_c	70°
Rx noise temperature	T	300 K
TIA resistor value	R_L	50 Ω
CP length	N_{CP}	2
DC-bias, ACO	$\mathscr{B}_{\text{DC(ACO)}}$	1.35 V
DC-bias, DCO	$\mathscr{B}_{\text{DC(DCO)}}$	1.50 V
Lower clipping	—	1.35 V
Upper clipping	—	1.65 V

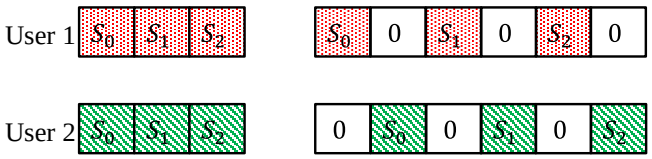

Fig. 6: Interleaved subcarrier mapping for the case of $\Gamma = 2$. Here, S_0, S_1, and S_2 refer to the symbols of each user.

where the $P_{\tau(elec)}$ is related to the optical transmit power $P_{\tau(opt)} = \eta P_{\tau(elec)}$ with η representing the LED electrical-to-optical power conversion efficiency.

The limited BW of the LED imposes restriction on the transmission BW per user, which depends on the signaling scheme used for the transmission. Given the M-QAM constellation, the maximum number of bits that can be transmitted per second, i.e., the spectral efficiencies of the ACO and DCO signaling for O-OFDMA schemes are [20]:

$$\xi_{\text{DCO}} = \frac{\log_2(M)\mathcal{M}}{N + N_{\text{CP}}}, \quad \xi_{\text{ACO}} = \frac{\log_2(M)\mathcal{M}}{2N + N_{\text{CP}}} \text{ (bps/Hz)}. \quad (9)$$

Remember that, N is the total number of subcarriers where $N = 2\mathcal{M} + 2$ with $\mathcal{M}$ the mapped subcarriers.

As ACO systems use just half of the subcarriers, their spectral efficiency is half that of the DCO scheme with the same modulation order and number of subcarriers. To compare DCO-based and ACO-based schemes reasonably, we adjust M accordingly to fix the spectral efficiency. The spectral efficiencies per user are then given by ξ_{DCO}/Γ and ξ_{ACO}/Γ,

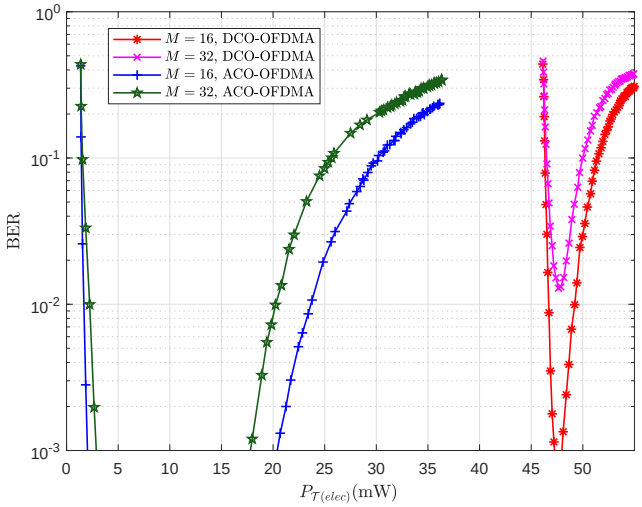

Fig. 7: BER performance comparison with respect to $P_{\tau(elec)}$ between DCO-OFDMA and ACO-OFDMA for fixed $\mathscr{E}_{b(\text{elec})/\mathscr{N}_o} = 15$ dB and BWs of ≈ 8 and 4 MHz for DCO, and ≈ 16 and 8 MHz for ACO signaling with 16-QAM and 32-QAM, respectively.

with the corresponding required BWs per user as:

$$\mathcal{B}_{\text{DCO}} = \frac{\mathscr{R}_b}{\xi_{\text{DCO}}/\Gamma} = \frac{\mathscr{R}_b\Gamma}{\xi_{\text{DCO}}}, \quad \mathcal{B}_{\text{ACO}} = \frac{\mathscr{R}_b\Gamma}{\xi_{\text{ACO}}}. \quad (10)$$

Now, given the $\mathcal{N}$ number of slots in a TMO-OFDMA scheme, the spectral efficiencies for the ACO and DCO signaling are:

$$\mathcal{B}_{\text{TM-DCO}} = \mathcal{N}\frac{\mathscr{R}_b\Gamma}{\xi_{\text{DCO}}}, \quad \mathcal{B}_{\text{TM-ACO}} = \mathcal{N}\frac{\mathscr{R}_b\Gamma}{\xi_{\text{ACO}}}. \quad (11)$$

B. Conventional O-OFDMA Scheme

1) Power Efficiency: In this section, we evaluate the electrical power efficiency in terms of the required electrical transmit power $P_{\tau(elec)}$ to achieve the target BER. To focus on the power efficiency performance of DCO and ACO signaling, we take into account the minimum channel attenuation, which occurs when all users are situated at the cell center, i.e., at $d = 0$ m. In this case, given $\Gamma = 16$, we set $\mathscr{M} = 16$, therefore $N = 514$ after imposing the HS. Then, with $\mathscr{R}_b = 1$ Mbps, Fig. 7 shows the BER performance versus $P_{\tau(elec)}$ for 16-QAM and 32-QAM for both DCO- and ACO-OFDMA, corresponding to the required transmission BWs $\mathcal{B}_{\text{DCO}} = 8$ and 4 MHz, and $\mathcal{B}_{\text{ACO}} = 16$ and 8 MHz, respectively. To make a fair comparison between the ACO and DCO signaling, here we vary $P_{\tau(elec)}$ for a fixed $\mathscr{E}_{b(\text{elec})/\mathscr{N}_o} = 15$ dB.

We can notice, the BER performance degrades with the increased QAM order due to the increasing clipping noise for both ACO and DCO signaling. As a matter of fact, DCO-OFDMA failed to reach the target BER with 32-QAM, whereas ACO-OFDMA requires approximately 45 mW less $P_{\tau(elec)}$ than DCO with 16-QAM. This is due to the relatively large $\mathscr{B}_{\text{DC}}$ in DCO-OFDMA and the resulting increased clipping noise. Also, for relatively large $P_{\tau(elec)}$, the increased clipping affects the BER performance, leading to BER of 0.5, if we increase the $P_{\tau(elec)}$ more (not shown in the figure).

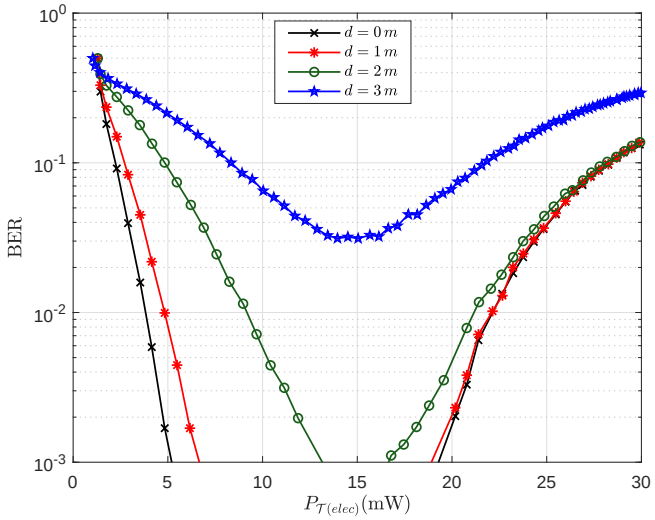

Fig. 8: BER versus $P_{\tau(elec)}$ performance of ACO-OFDMA scheme for different distance d of the desired user with $M = 16$, where the other 15 users located at the same position as the desired user.

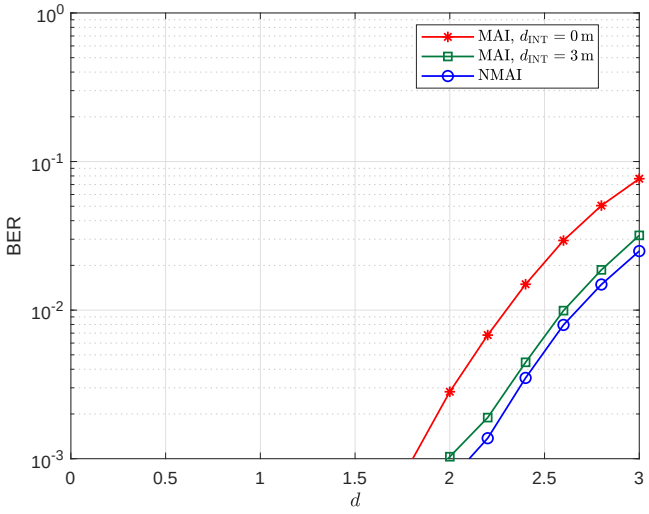

Fig. 9: BER versus desired user distance d.

2) BER Performance: Given the relatively low transmit power requirement and the limited clipping noise effect, lets focus on the ACO-OFDMA scheme as an appropriate scheme, as shown in the Fig. 7. Considering the 16-QAM constellation because of being least affected by clipping noise, we present BER versus $P_{\tau(elec)}$ in Fig.8 for different distance d of the desired user. Here, all users are at the same position and changing distance d with the desired user. As expected, with the increasing distance of the desired user the BER performance degrades due to the channel attenuation. We notice that for each d distance, the least BER is achieved when $P_{\tau(elec)} = 15\,\text{mW}$.

3) MAI Effect: Now, in order to see the MAI effect we set $P_{\tau(elec)} = 15\,\text{mW}$, which has been shown in Fig. 8 as optimal $P_{\tau(elec)}$ to achieve the target BER. Figure 9 presents the BER performance results where we change the desired user distance d form cell center to the edge for both MAI and NMAI case. Here, NMAI refers to the No MAI, i.e., only a single user is present in the scenario. For the case of NMAI, as expected, with the increasing d, the BER degrades due to the increased channel attenuation. For the case of MAI, we study two scenarios where the other (i.e., interfering) users are positioned at $d = 0\,\text{m}$ and $d = 3\,\text{m}$, respectively. Let us define the interfering users' distance as d_{INT}, as shown in Fig. 9. We can notice the worst MAI when $d_{\text{INT}} = 0\,\text{m}$. However, the MAI effect is observed to be less for $d_{\text{INT}} = 3$,m. This is in-fact so called "near-far" problem caused by MAI, where the strongest signals of interfering users at the cell center have the most MAI effect, as compared to the weakest interferers at the cell edge. This is because of the clipping noise resulting in *spectral regrowth* in the adjacent subcarriers resulting in inter-carrier-interference [23].

C. TMO-OFDMA

1) MAI Effect: Here, we apply our proposed TMO-OFDMA scheme for the worst case MAI scenario as in the previous subsection. Focusing on the ACO signaling due to its energy efficiency, we compare the BER performance between the ACO-OFDMA and TM-ACO-OFDMA. For the TM-ACO-OFDMA, we transmit a group of users data into their dedicated two different time slots denoted by t_{SLOT1} and t_{SLOT2}, each with $\Gamma = 8$ users, as shown in Fig. 10. For each slot, we consider the same $\mathcal{M} = 256$ as for the ACO-OFDMA, where the unallocated subcarriers are replaced by zeros, resulting in $\xi_{\text{DCO}} = 0.5$ for 16-QAM. Therefore, in order to transmit data at the same rate as the ACO-OFDMA scheme, the required BW per slot for TMO-ACO-OFDMA is $\mathcal{B}_{\text{TM-ACO}} = 32\,\text{MHz}$. Figure 11 shows the BER performance result for ACO-OFDMA and TMO-ACO-OFDMA for both MAI and NMAI case. We notice a substantial improvement in MAI performance for the case of TMO-ACO-OFDMA, as compared to the ACO-OFDMA. In fact, MAI has negligible effect on the performance of TMO-ACO-OFDMA scheme. This is due to the padded zeros in between the adjacent sub-carriers, resulting in reduced inter-carrier-interference caused by clipping noise. Moreover, the number of users per slot was limited to 8, reducing the MAI effect.

V. Computational Complexity

The computational complexity of IFFT/FFT is realized in terms of floating-point operations (FLOPs) related to its real additions and multiplications [42]. We analyze the computational cost of the considered schemes based on N-point IFFT/FFT for N number of mapped subcarriers. The use of Cooley-Tukey method in developing a higher-order radix IFFT/FFT algorithm is relatively more efficient in terms of FLOP count [43]. Furthermore, the development of split-radix algorithms, e.g., the radix-2/4 and radix 2/8, achieved a better FLOP count [42, 44]. Without loss of generality, we simply consider a radix-2 algorithm, where a N-point FFT/IFFT

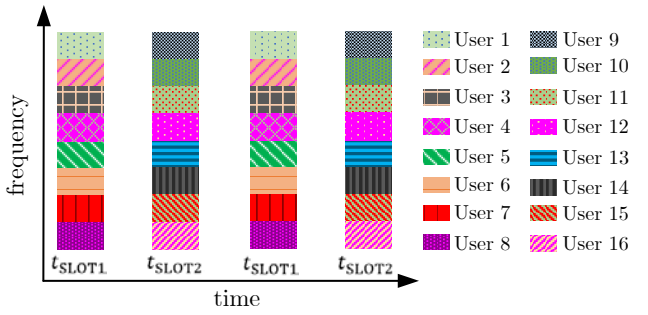

Fig. 10: Allocation of 16 users in two different time slots for TMO-OFDMA. Here, t_{SLOT1} and t_{SLOT2} correspond to the time slots for user 1 to 8 and user 9 to 16, respectively.

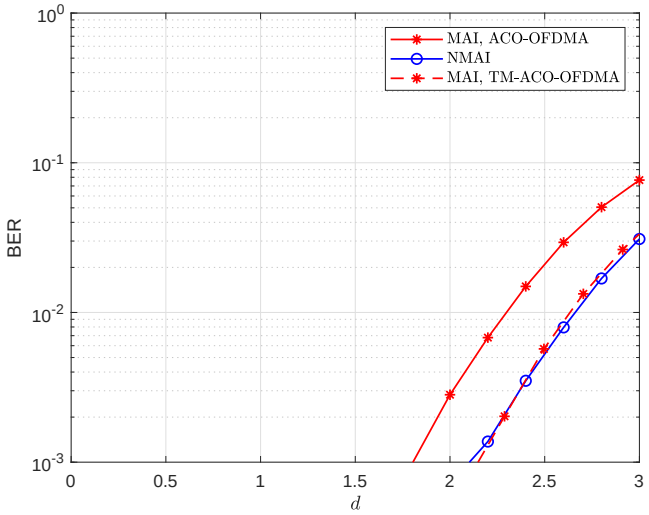

Fig. 11: MAI performance comparison in terms of BER in between the ACO-OFDMA and TM-ACO-OFDMA. Here, MAI refers to the case where the desired user changes its position from the cell center to the edge and the other 15 users are located at the cell center.

requires approximately $5Nlog_2(N)$ arithmetic operations [43]. For TMO-OFDMA, the FLOP count, i.e., computational complexity, reduced to a factor of 2 due to the inserted zeros in the adjacent subcarriers. An example of radix-2 algorithm for TMO-OFDMA considering DCO signaling with $N = 8$ is shown in Fig. 12. Given zeros in both of the symbols in a butterfly of length 2 and a zero in one of the symbols, no arithmetic operation is required. At Stage-1, symbols with zeros produce an identical copy of the result obtained by precedent non-zero symbols at Stage-3. As a result, no arithmetic operation is required for symbols containing zeros, lowering the computational cost of TMO-OFDMA by a factor of 2.

Table II shows the computational complexity of the studied ACO signaling at the Tx and Rx for O-OFDMA and TMO-OFDMA schemes. Remember that the ACO schemes require twice the subcarriers as DCO schemes.

Now, we study the computational complexity of the considered ACO schemes. Figure 13 shows the complexity analysis

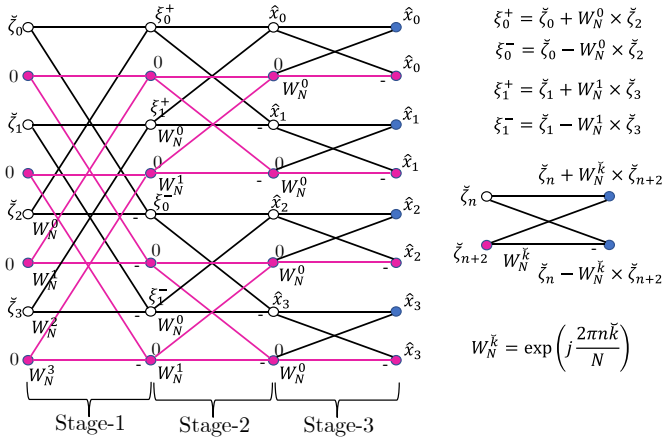

Fig. 12: Illustration of a radix-2 FFT algorithm for DCO signaling with $N = 8$ in TMO-OFDMA. $W_n^{\check{k}}$ refers to the so-called *twiddle factor* [45].

TABLE II: Computational Complexity of considered schemes for ACO signaling.

MA Scheme	Tx	Rx
ACO-OFDMA	$10N\log_2(2N)$	$10N\log_2(N)$
TM-ACO-OFDMA	$5N\log_2(2N)$	$10N\log_2(2N)$

results in terms of FLOP count at the Tx. We focus on the Tx side since it affects the battery lifetime of mobile IoT devices. As expected, the number of FLOPs increases with the increased number of subcarriers N. Moreover, TMO-ACO-OFDMA outperforms ACO-OFDMA by a factor of 2 in terms of the number of FLOPs required.

VI. Conclusion

We proposed a time scheduling based TMO-OFDMA scheme by transmitting group of O-OFDMA users' data in

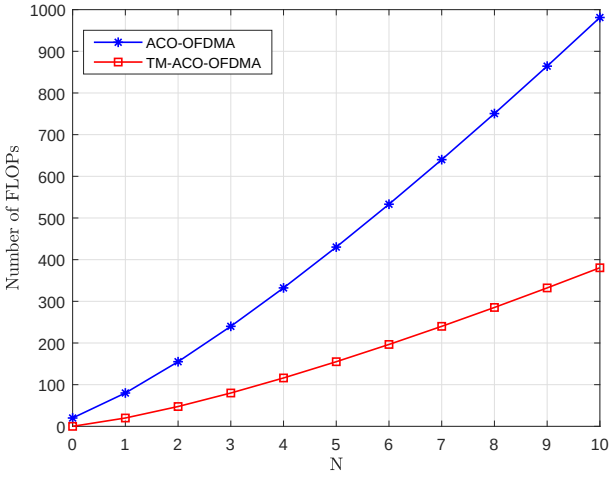

Fig. 13: Complexity analysis of ACO-OFDMA and TM-ACO-OFDMA.

their dedicated time slots for the LiFi-based uplink IoT networks in an indoor scenario. We studied the energy efficiency of ACO and DCO signaling and demonstrated the advantage of ACO signaling in achieving target BER with relatively low transmit power by quite a large margin. Taking into account realistic LED characteristics, we studied the MAI performance of our proposed TMO-OFDMA scheme compared to its O-OFDMA counterparts. In particular, we demonstrated the effectiveness of our scheme in reducing MAI, albeit with the requirement of increased transmission BW. We further showed that our proposed scheme can significantly reduce Tx energy consumption for IoT devices compared to the O-OFDMA scheme, thanks to the reduced computational complexity of TMO-OFDMA.

As for future research direction, it would be interesting to analyze the performance of the scheme for random Tx orientation during mobility, particularly for on-body IoT devices. Moreover, for a large-size indoor space, multiple AP arrangements should be employed, which requires the development of efficient time synchronization techniques for APs and handover protocols for multi-cell architecture.

REFERENCES

[1] L. Qian, R. Zhao, H. Zhang, J. Lu, and W. Wu, "Cooperative bargaining game-based scheduling model with variable multiobjective weights in a UWB and 5G embedded workshop," *IEEE Internet of Things Journal*, vol. 9, no. 11, pp. 8498–8514, June 2022.

[2] N. Alam and M. A. Rahman, "A survey into COVID-19 induced pneumonia detection and feasibility of using UWB medical imaging," *AIUB Journal of Science and Engineering*, vol. 20, no. 3, pp. 77–86, Sep. 2021.

[3] M. J. Hasan, "Multi-user data transmission in optical wireless body-area networks for medical applications," Theses, Ecole Centrale Marseille, Nov. 2021. [Online]. Available: https://theses.hal.science/tel-03873596

[4] H. Haas, "LiFi is a paradigm-shifting 5G technology," *Reviews in Physics*, vol. 3, pp. 26–31, Jan. 2018.

[5] M. Giordani, M. Polese, M. Mezzavilla, S. Rangan, and M. Zorzi, "Toward 6G networks: Use cases and technologies," *IEEE Communications Magazine*, vol. 58, no. 3, pp. 55–61, Mar. 2020.

[6] N. Chi, Y. Zhou, Y. Wei, and F. Hu, "Visible light communication in 6G: Advances, challenges, and prospects," *IEEE Vehicular Technology Magazine*, vol. 15, no. 4, pp. 93–102, 2020.

[7] Z. Ghassemlooy, L. N. Alves, S. Zvanovec, and M. A. Khalighi, Eds., *Visible Light Communications: Theory and Applications*. CRC-Press, 2017.

[8] R. Badeel, S. K. Subramaniam, Z. M. Hanapi, and A. Muhammed, "A review on LiFi network research: Open issues, applications and future directions," *Applied Sciences*, vol. 11, no. 23, 2021.

[9] IEC-62471, "Photobiological safety of lamps and lamp systems," International Electrotechnical Commission, Geneva, Switzerland, Standard, 2008.

[10] Z. Chen, Z. Ding, X. Dai, and R. Zhang, "An optimization perspective of the superiority of NOMA compared to conventional OMA," *IEEE Transactions on Signal Processing*, vol. 65, no. 19, pp. 5191–5202, 2017.

[11] H. Abumarshoud, H. Alshaer, and H. Haas, "Dynamic multiple access configuration in intelligent LiFi attocellular access points," *IEEE Access*, vol. 7, pp. 62 126–62 141, 2019.

[12] M. J. Hasan, M. A. Khalighi, and B. Béchadergue, "Experimental implementation of Optical-CDMA for medical Extra-WBAN links," in *12th International Symposium on Communication Systems, Networks and Digital Signal Processing (CSNDSP)*, July 2020, Porto, Portugal.

[13] M. J. Hasan, M. A. Khalighi, J. García-Márquez, and B. Béchadergue, "Performance analysis of optical-CDMA for uplink transmission in medical extra-WBANs," *IEEE Access*, vol. 8, pp. 171 672–171 685, Sept. 2020.

[14] D. R. Dhatchayeny, S. Arya, and Y. H. Chung, "Infrared-based multiple-patient monitoring in indoor optical wireless healthcare systems," *IEEE Sensors Journal*, vol. 19, no. 14, pp. 5594–5599, July 2019.

[15] W. C. Yang, G.-C; Kwong, "Performance analysis of optical CDMA with prime codes," *Electronics Letters*, vol. 33, no. 7, pp. 569–570, Mar. 1995.

[16] D. Tagliaferri and C. Capsoni, "High-speed wireless infrared uplink scheme for airplane passengers' communications," *Electronics Letters*, vol. 53, no. 13, pp. 887–888, June 2017.

[17] C. Chen, S. Fu, X. Jian, M. Liu, X. Deng, and Z. Ding, "NOMA for energy-efficient LiFi-enabled bidirectional IoT communication," *IEEE Transactions on Communications*, vol. 69, no. 3, pp. 1693–1706, Jan. 2021.

[18] M. Shirvanimoghaddam, M. Dohler, and S. J. Johnson, "Massive non-orthogonal multiple access for cellular IoT: Potentials and limitations," *IEEE Communications Magazine*, vol. 55, no. 9, pp. 55–61, Sept. 2017.

[19] Z. Liu and L.-L. Yang, "Sparse or dense: A comparative study of code-domain NOMA systems," *IEEE Transactions on Wireless Communications*, vol. 20, no. 8, pp. 4768–4780, Mar. 2021.

[20] J. Armstrong, "OFDM for optical communications," *Journal of Lightwave Technology*, vol. 27, no. 3, pp. 189–204, Feb. 2009.

[21] S. D. Dissanayake and J. Armstrong, "Comparison of ACO-OFDM, DCO-OFDM and ADO-OFDM in IM/DD systems," *Journal of Lightwave Technology*, vol. 31, no. 7, pp. 1063–1072, Apr. 2013.

[22] X. Li, J. Vucic, V. Jungnickel, and J. Armstrong, "On the capacity of intensity-modulated direct-detection systems and the information rate of aco-ofdm for indoor optical wireless applications," *IEEE Transactions on Communications*, vol. 60, no. 3, pp. 799–809, Mar. 2012.

[23] M. J. Hasan, M. A. Khalighi, V. Jungnickel, L. N. Alves, and B. Béchadergue, "An energy-efficient optical wireless OFDMA scheme for medical body-area networks," *IEEE Transactions on Green Communications and Networking*, vol. 6, no. 3, pp. 1806–1818, Sep. 2022.

[24] W.-W. Hu, "SLM-based ACO-OFDM VLC system with low-complexity minimum amplitude difference decoder," *Electronics Letters*, vol. 54, pp. 144–146, Feb. 2018.

[25] W. O. Popoola, Z. Ghassemlooy, and B. G. Stewart, "Pilot-assisted PAPR reduction technique for optical OFDM communication systems," *Journal of Lightwave Technology*, vol. 32, no. 7, pp. 1374–1382, Feb. 2014.

[26] H. G. Myung and D. J. Goodman, *Single Carrier FDMA*. Wiley, 2008, pp. 37–59.

[27] C. Chen, D. A. Basnayaka, and H. Haas, "Downlink performance of optical attocell networks," *Journal of Lightwave Technology*, vol. 34, no. 1, pp. 137–156, Jan. 2016.

[28] T. Wu, F. Wu, J. Redouté, and M. R. Yuce, "An autonomous wireless body area network implementation towards IoT connected healthcare applications," *IEEE Access*, vol. 5, pp. 11 413–11 422, June 2017.

[29] R. Cavallari, F. Martelli, R. Rosini, C. Buratti, and R. Verdone, "A survey on wireless body area networks: Technologies and design challenges," *IEEE Communications Surveys & Tutorials*, vol. 16, no. 3, pp. 1635–1657, Mar. 2014.

[30] *DS190 LUXEON IR Compact Line Product Datasheet*, Lumileds Holding B.V., 2018.

[31] M. J. Hasan, M. Ali Khalighi, L. N. Alves, and B. Béchadergue, "Impact of synchronization errors on the performance of ACO-OFDMA signaling for medical extra-WBAN links," in *2021 IEEE 32nd Annual International Symposium on Personal, Indoor and Mobile Radio Communications (PIMRC)*, Sept. 2021, pp. 1–6, Helsinki, Finland.

[32] M. Morelli, L. Sanguinetti, and H. V. Poor, "A robust ranging scheme for OFDMA-based networks," *IEEE Transactions on Communications*, vol. 57, no. 8, pp. 2441–2452, Aug. 2009.

[33] S. Tian, K. Panta, H. A. Suraweera, B. J. C. Schmidt, S. McLaughlin, and J. Armstrong, "A novel timing synchronization method for -OFDM-based optical wireless communications," *IEEE Transactions on Wireless Communications*, vol. 7, no. 12, pp. 4958–4967, Dec. 2008.

[34] Y. Jiang, Y. Wang, P. Cao, M. Safari, J. Thompson, and H. Haas, "Robust and low-complexity timing synchronization for DCO-OFDM LiFi systems," *IEEE Journal on Selected Areas in Communications*, vol. 36, no. 1, pp. 53–65, Jan. 2018.

[35] T.-A. Truong, M. Arzel, H. Lin, B. Jahan, and M. Jezequel, "New low-complexity and robust time synchronization technique for optical IMDD OFDM transmissions," *Opt. Express*, vol. 22, no. 12, pp. 14 322–14 340, June 2014.

[36] X. Qian, Y. Deng, H. Deng, Y. Hu, C. Zhang, and J. Du, "Synchronisation algorithm based on zero correlation code pair for OFDM-based VLC systems," *IET Communications*, vol. 11, no. 2, pp. 205–210, Jan. 2017.

[37] J. M. Kahn, W. J. Krause, and J. B. Carruthers, "Experimental characterization of non-directed indoor infrared channels," *IEEE Transactions on Communications*, vol. 43, no. 2/3/4, pp. 1613–1623, Feb. 1995.

[38] J. M. Kahn and J. R. Barry, "Wireless infrared communications," *Proceedings of the IEEE*, vol. 85, no. 2, pp. 265–298, Feb. 1997.
[39] Z. Ghassemlooy, W. Popoola, and S. Rajbhandari, *Optical Wireless Communications: System and Channel Modelling with MATLAB*, 2nd ed. CRC Press, Inc., 2019.
[40] F. Xu, M. Khalighi, and S. Bourennane, "Impact of different noise sources on the performance of PIN- and APD-based FSO receivers," in *International Conference on Telecommunications (ConTel)*, June 2011, pp. 211–218, Graz, Austria.
[41] *HDN1102W-TR Standard Product Specifications*, Stanley Electric Co. Ltd., 2014.
[42] W. Zheng, K. Li, and K. Li, "Scaled radix-2/8 algorithm for efficient computation of length-$N = 2^m$ DFTs," *IEEE Transactions on Signal Processing*, vol. 62, no. 10, pp. 2492–2503, Mar. 2014.
[43] J. Cooley and J. Tukey, "An algorithm for the machine calculation of complex Fourier series," *Mathematics of Computation*, vol. 19, no. 90, pp. 297–301, 1965.
[44] S. Bouguezel, M. O. Ahmad, and M. N. S. Swamy, "A general class of split-radix FFT algorithms for the computation of the DFT of length-2^m," *IEEE Transactions on Signal Processing*, vol. 55, no. 8, pp. 4127–4138, July 2007.
[45] A. V. Oppenheim and R. W. Schafer, *Discrete-Time Signal Processing*, 3rd ed. USA: Prentice Hall Press, 2009.

BIOGRAPHY

Md Jahid Hasan (Member, IEEE) received the Ph.D. degree for his work on multi-user data transmission in optical wireless body area networks for medical applications from the École Centrale de Marseille, France, in 2021, and the joint international M.Sc. degree in smart systems integration from Heriot-Watt-University, Edinburgh, U.K., in 2016. His Ph.D. thesis work was funded by the European Union's Marie Sklodowska-Curie Vision ITN Project. Since 2022, he is serving as an Assistant Professor with the Department of Electrical and Electronic Engineering (EEE), American International University-Bangladesh (AIUB), Dhaka, Bangladesh. Currently, he is conducting postdoctoral research in University College Cork, Tyndall National Institute, Ireland.

From 2012 to 2014, he worked as an ASIC Design Engineer with Fastrack Anontex Ltd., Dhaka. He also served as a Lecturer with the Department of EEE, AIUB from 2017 to 2018. From 2018 to 2021, he worked as an Early-Stage Researcher with the Vision ITN Project hosted by Oledcomm SAS, Paris, France. His research interests include optical wireless communications, digital signal processing, and FPGA-based implementation. He was also a recipient of the Erasmus Mundus scholarship during his two years M.Sc. Program from 2014 to 2016.

Ikenna Chinazaekpere Ijeh (Member, IEEE) is from Abakaliki, Ebonyi State, southeastern Nigeria. He received the B.Eng. degree in electrical electronics engineering from Caritas University, Enugu, Nigeria, in 2013, the M.Sc. degree in control and instrumentation from the University of Derby, Derby, United Kingdom, in 2016, and the Ph.D. degree in optics, photonics and image processing from École Centrale de Marseille, France, in 2021. He is currently a Lecturer with the Department of Electrical and Electronic Engineering, Alex-Ekwueme Federal University Ndufu-Alike Ikwo, Ebonyi State, Nigeria. His research interests include wireless communication systems and automation of control systems.

Oussama Haddad received his B.Sc. and M.Sc. degrees in electrical engineering from National Polytechnic School of Algiers, Algeria, in 2017, and his Ph.D. from Fresnel Institute, École Centrale Marseille, France, in 2021. He is currently working as a research and teaching assistant at the Microelectronics and Telecommunications Department of Polytech-Marseille, France. His research interests include optical wireless communications and wireless body area networks.

Md Abdur Rahman (Senior Member, IEEE) is an experienced Researcher with a demonstrated history of working in the higher education industry. He has extensive knowledge of radio frequency (RF), wireless communication, biomedical imaging, machine learning, and antenna propagation. Profound research professional with Doctor of Philosophy (Ph.D.) from Tokyo Institute of Technology University in 2013 focused on software defined radio (SDR) and has experience as a Postdoctoral Researcher in Federation University Australia from 2014, focused on Application of modern signal processing techniques in gene expressions to form gene regulatory network. His research interest is focused on RF/microwave circuits and systems, digital signal processing, biomedical image processing, nano-electronics, machine learning, wireless communication, antenna propagation. Currently, he is working as a Pro Vice-Chancellor at American International University-Bangladesh (AIUB) and a Professor in the department of Electrical and Electronic Engineering, AIUB.